

Research on the steam–gas pressurizer model with Relap5 code

Xi-Zhen Ma¹ · Hai-Jun Jia¹ · Yang Liu¹

Received: 21 August 2015 / Revised: 11 December 2015 / Accepted: 18 December 2015 / Published online: 28 March 2017
© Shanghai Institute of Applied Physics, Chinese Academy of Sciences, Chinese Nuclear Society, Science Press China and Springer Science+Business Media Singapore 2017

Abstract Steam–gas pressurizers are self-pressurizing, and since steam and noncondensable gas are used to sustain their pressure, they experience very complicated thermal–hydraulic phenomena owing to the presence of the latter. A steam–gas pressurizer model was developed using Relap5 code to investigate such a pressurizer’s thermal–hydraulic characteristics. The important thermal–hydraulic processes occurring in the pressurizer model include bulk flashing, rainout, wall condensation with noncondensable gas, and interfacial heat and mass transfer. The pressurizer model was verified using results from insurge experiments performed at the Massachusetts Institute of Technology. It was found that noncondensable gas was one of the important factors governing the pressure response, and the accuracy of the developed model would change with different mass fractions and types of noncondensable gas.

Keywords Relap5 code · Noncondensable gas · Heat and mass transfer · Steam–gas pressurizer · Condensation

List of symbols

A	Area (m^2)
B	Body force (m/s^2)
C	Coefficient of virtual mass
D	Diameter (m)
Di	Energy-dissipation function (W/m^3)
F	Drag coefficient ($\text{m}^3/\text{kg s}$)

f_c	Modification factor
H	Volumetric heat-transfer coefficient (W/K m^3)
h	Specific enthalpy (J/kg)
h_c	Condensation heat-transfer coefficient with noncondensable gas ($\text{W}/(\text{m}^2 \text{K})$)
h_l	Dittus–Boelter coefficient assuming all fluid is liquid ($\text{W}/(\text{m}^2 \text{K})$)
h_{sf}	Superficial heat-transfer coefficient ($\text{W}/(\text{m}^2 \text{K})$)
k	Thermal conductivity (W/m K)
M	Mass (kg)
P	Pressure (Pa)
Pr	Prandtl number
P_{red}	Reduced bulk pressure (Pa)
Q	Volumetric heat rate (W/m^3)
Re	Reynolds number
T	Temperature (K)
t	Time (s)
U	Specific internal energy (J/kg)
v	Velocity (m/s)
X	Mass fraction
Z	Two-phase friction correlation factor

Symbols

α	Void fraction
Γ	Volumetric mass exchange rate ($\text{kg}/\text{m}^3 \text{ s}$)
ε	Coefficient
ρ	Density (kg/m^3)

Subscripts

cr	Critical condition
f	Liquid phase
g	Gas phase
h	Hydraulic
i	Interface

✉ Xi-Zhen Ma
cnst_xizhen@163.com

¹ Institute of Nuclear and New Energy Technology, Collaborative Innovation Center of Advanced Nuclear Energy Technology, Key Laboratory of Advanced Reactor Engineering and Safety of Ministry of Education, Tsinghua University, Beijing 100084, China

liq	Liquid phase
m	Mixture of gas phase and liquid phase
mix	Mixture of vapor and noncondensable gas
n	Noncondensable gas
ref	Reference condition
s	Steam component of gas phase
w	Wall

Superscripts

- * Total derivative of saturation property with respect to pressure
- ' Derivative

1 Introduction

Small and medium nuclear reactors with low capital costs, high performance, and enhanced safety are widely used in district heating, seawater desalination, and ship propulsion and are usually developed as integral reactors. Since steam–gas pressurizers are self-pressurizing and can minimize the use of active devices, such as heaters and sprayers, they are widely applied in such reactors, e.g., NHR-II (Nuclear Heating Reactor-II) [1], REX-10 (Regional Energy Reactor; 10MW_{th}), SMART (System-Integrated Modular Advanced Reactor) [2].

The thermal–hydraulic characteristics of a steam–gas pressurizer are considered the most important factors that affect the safe operation of small and medium reactors. However, studies on such pressurizers have been rarely done since reactors with a steam–gas pressurizer have not been commercialized, and the available information on such research is extremely restricted. The analysis code GARRIC was developed by Russian researchers to investigate the characteristics of steam–gas pressurizers [3] and the distribution of noncondensable gas, and some experiments have been conducted to verify GARRIC. Unfortunately, the results of the experiments are not available. In order to investigate the effect of a noncondensable gas on a steam–gas pressurizer, experiments were performed at the Massachusetts Institute of Technology [4] in which changes of pressure in the pressurizer were observed for different mass fractions of and types of noncondensable gas. Kim and Griffith [5] noted that condensation heat transfer at the wall played an important role in determining the pressure transient in a steam–gas pressurizer and that the presence of even a small amount of noncondensable gas would lead to a significant reduction in heat transfer during condensation. Murase et al. [6] proposed that the condensation heat-transfer coefficient was a function of the steam/gas ratio. A theoretical pressurizer model was developed by Kim [7] and used in RETRAN-3D/TNT code.

In this study, a steam–gas pressurizer model was developed to investigate the thermal–hydraulic characteristics of a steam–gas pressurizer using Relap5 code. Apart from the general conservation equations [8–10], the model includes an interfacial heat- and mass-transfer model and a wall film condensation model with the presence of noncondensable gas. The noncondensable gas plays a key role in the thermal–hydraulic processes occurring in the pressurizer since different types of and mass fractions of noncondensable gas account for significant differences in the pressure transients in the steam–gas pressurizer. The results of this study have been verified with those from pressurizer insurge experiments performed at Massachusetts Institute of Technology (MIT).

2 Pressurizer physical model

In this study, a steam–gas pressurizer's volume is divided into three regions based on phase conditions: a steam/gas region, a steam/liquid interfacial region, and a liquid region [11], as shown in Fig. 1. Region 1 is the gas-mixture region including vapor, noncondensable gas, and liquid droplets. Region 2 is the steam and liquid interfacial region in which the processes of heat and mass transfer occur. Region 3 is the saturated liquid region containing rising bubbles.

The governing equations of the model include the phase-continuity, momentum-conservation, and energy-conservation equations [12]. The presence of noncondensable gas is the most important phenomenon in the pressurizer, and it is thus necessary to consider its effect when solving these governing equations.

The following assumptions are made in the model:

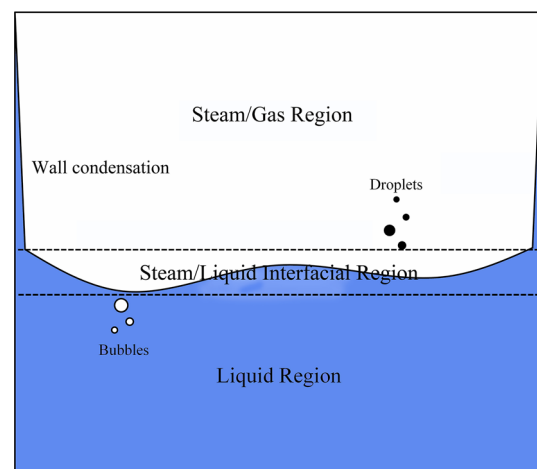


Fig. 1 Theoretical model of integrated gas–steam pressurizer

1. Vapor and noncondensable gas in the steam/gas region are fully mixed and share the same temperature.
2. Liquid droplets in the steam/gas region are saturated before reaching the liquid.
3. Each region can have different temperatures, and the three regions have the same pressure.
4. Each region has the same enthalpy at each time step.
5. The total volume of the steam–gas pressurizer is constant.

The mass-conservation equations are written as

$$\frac{\partial}{\partial t}(\alpha_g \rho_g) + \frac{1}{A} \frac{\partial}{\partial x}(\alpha_g \rho_g v_g A) = \Gamma_g, \tag{1}$$

$$\frac{\partial}{\partial t}(\alpha_f \rho_f) + \frac{1}{A} \frac{\partial}{\partial x}(\alpha_f \rho_f v_f A) = \Gamma_f, \tag{2}$$

$$\frac{\partial}{\partial t}(\alpha_g \rho_g X_n) + \frac{1}{A} \frac{\partial}{\partial x}(\alpha_g \rho_g v_g X_n A) = 0. \tag{3}$$

The mass-governing equations include gas-phase, liquid-phase, and noncondensable-gas-phase equations. X_n is defined as the mass fraction of noncondensable gas based on the mass of the gas-mixture phase, and it is assumed that all properties of the gas phase are mixture properties of the steam/noncondensable-gas mixture, where

$$X_n = \frac{M_n}{M_n + M_s}. \tag{4}$$

Since the noncondensable gas is assumed to be in mechanical and thermal equilibrium with the vapor phase in the model, the gas phase shares the same velocity and temperature; that is, $v_n = v_g$, and $T_n = T_g$. Without considering the mass dissipation, the total mass of the gas and liquid phases is constant, so the liquid generation term is the negative of the vapor generation term; that is, $\Gamma_g = -\Gamma_f$.

It is further assumed that, in the interfacial mass-transfer model [13], the total mass transfer (Γ_g) can be partitioned into the mass transfer at the steam/liquid interface in the bulk fluid (Γ_{ig}) and the mass transfer at the steam/liquid interface in the boundary layer near the walls (Γ_w); that is,

$$\Gamma_g = \Gamma_{ig} + \Gamma_w. \tag{5}$$

The mass-transfer term Γ_w is evaluated as

$$\Gamma_w = h_m \rho_s \ln \left(\frac{P - P_{vi}}{P - P_v} \right). \tag{6}$$

The momentum-conservation equations are written with the following simplifications:

1. The Reynolds stresses are neglected.
2. The phase pressures are assumed to be equal, and the interfacial pressures are equal to the phase pressures.
3. The interfacial momentum storage and phase viscous stresses are neglected.

4. The interface force terms consist of both pressure and viscous stresses.

We thus write

$$\begin{aligned} \alpha_g \rho_g A \frac{\partial v_g}{\partial t} + \frac{1}{2} \alpha_g \rho_g A \frac{\partial v_g^2}{\partial x} &= -\alpha_g A \frac{\partial P}{\partial x} + \alpha_g \rho_g B_x A \\ &- (\alpha_g \rho_g A) f_{wg}(v_g) + \Gamma_g A (v_{gi} - v_g) - (\alpha_g \rho_g A) f_{ig}(v_g - v_f) \\ &- C \alpha_g \alpha_f \rho_m A \left[\frac{\partial (v_g - v_f)}{\partial t} + v_f \frac{\partial v_g}{\partial x} - v_g \frac{\partial v_f}{\partial x} \right], \end{aligned} \tag{7}$$

$$\begin{aligned} \alpha_f \rho_f A \frac{\partial v_f}{\partial t} + \frac{1}{2} \alpha_f \rho_f A \frac{\partial v_f^2}{\partial x} &= -\alpha_f A \frac{\partial P}{\partial x} + \alpha_f \rho_f B_x A \\ &- (\alpha_f \rho_f A) f_{wf}(v_f) + \Gamma_g A (v_{fi} - v_f) - (\alpha_f \rho_f A) f_{if}(v_f - v_g) \\ &- C \alpha_f \alpha_g \rho_m A \left[\frac{\partial (v_f - v_g)}{\partial t} + v_g \frac{\partial v_f}{\partial x} - v_f \frac{\partial v_g}{\partial x} \right]. \end{aligned} \tag{8}$$

The momentum equations are unchanged when a noncondensable gas is present. f_{wg}/f_{wf} is the wall drag coefficient and f_{ig}/f_{if} is the interphase drag coefficient for the gas/liquid [14]. The gas-phase properties are evaluated for the steam/noncondensable-gas mixture in all of the equations.

The energy-conservation equations are written as

$$\begin{aligned} \frac{\partial}{\partial t}(\alpha_g \rho_g U_g) + \frac{1}{A} \frac{\partial}{\partial x}(\alpha_g \rho_g U_g v_g A) \\ &= -P \frac{\partial \alpha_g}{\partial t} - \frac{P}{A} \frac{\partial}{\partial x}(\alpha_g v_g A) + Q_{wg} + Q_{ig} + \Gamma_{ig} h_g^* + \Gamma_w h'_g \\ &- Q_{gf} + D i_g, \end{aligned} \tag{9}$$

$$\begin{aligned} \frac{\partial}{\partial t}(\alpha_f \rho_f U_f) + \frac{1}{A} \frac{\partial}{\partial x}(\alpha_f \rho_f U_f v_f A) \\ &= -P \frac{\partial \alpha_f}{\partial t} - \frac{P}{A} \frac{\partial}{\partial x}(\alpha_f v_f A) + Q_{wf} + Q_{if} + \Gamma_{if} h_f^* + \Gamma_w h'_f \\ &- Q_{gf} + D i_f. \end{aligned} \tag{10}$$

The term Q_{gf} in the above equations is defined as the sensible heat-transfer rate unit volume at the noncondensable-gas–liquid interface and is given by

$$Q_{gf} = \frac{P_n}{P} H_{gf} (T_g - T_f). \tag{11}$$

The phase-wall heat-transfer rates per unit volume Q_{wg} and Q_{wf} are defined as

$$Q_{wg} = H_g (T_w - T_{refg}) \quad Q_{wf} = H_f (T_w - T_{reff}). \tag{12}$$

The interfacial heat-transfer (Q_{ig}) and mass-transfer (Γ_{ig}) terms must be modified because of the presence of a noncondensable gas; that is,

$$Q_{ig} = \frac{P_s}{P} H_{ig} (T_s - T_g) - \left(\frac{1 - \varepsilon}{2} \right) \Gamma_w (h'_g - h'_f), \tag{13}$$

$$\Gamma_{ig} = -\Gamma_{if} = -\frac{\frac{P_s}{P} H_{ig}(T_s - T_g) + H_{if}(T_s - T_f)}{h_g^* - h_f^*}, \quad (14)$$

where h_g^* is the steam enthalpy based on the partial pressure of steam instead of the total pressure. The phase energy-dissipation terms Di_g/Di_f are decided by wall friction and pump effects. However, the dissipation effects due to interface mass transfer, interface friction, and virtual mass are neglected in the energy equations [15–17]. The dissipation effects are given as

$$Di_g = \alpha_g \rho_g f_{wg} v_g^2, \quad Di_f = \alpha_f \rho_f f_{wf} v_f^2. \quad (15)$$

We next consider wall condensation with a noncondensable gas and note that condensation heat transfer at the wall plays a key role in determining the pressure transient in the steam–gas pressurizer. The following assumptions apply to our condensation model [18]:

1. The sensible heat transfer through the diffusion layer to the interface is negligible.
2. The gas is not removed from the vapor region by dissolving it in the condensate.
3. Stratification of the noncondensable gas in steam by buoyancy effects is negligible.

The condensation heat and mass transfer are evaluated by Shah’s correlations [19] as follows:

$$h_c = h_{sf} \left(1 + \frac{3.8}{Z^{0.95}} \right), \quad Z = \left(\frac{1}{X_m} - 1 \right)^{0.8} P_{red}^{0.8}, \quad (16)$$

$$h_{sf} = h_l (1 - X_m)^{0.8}, \quad h_l = 0.023 \left(\frac{k_f}{D_h} \right) Re_f^{0.8} Pr_f^{0.4}, \quad (17)$$

$$Re_f = \frac{\rho_f v D}{\mu_f}, \quad Pr_f = \frac{\mu_f C_p}{k}$$

where P_{red} is the reduced bulk pressure; that is, $P_{red} = P/P_{cr}$. X is the gas-mixture (including steam and noncondensable gas) mass fraction in the pressurizer, where

$$X_m = \frac{M_{mix}}{M_{mix} + M_{liq}}. \quad (18)$$

The effects of noncondensable gas are represented by multipliers that modify and reduce the heat-transfer coefficient. The modification factor is f_c , which is derived from the Vierow–Schrock correlation [20]:

$$f_c = \begin{cases} 1 - 10X_n, & X_n < 0.063 \\ 1 - 0.938X_n^{0.13}, & 0.063 \leq X_n \leq 0.60 \\ 1 - X_n^{0.13}, & X_n > 0.60 \end{cases}. \quad (19)$$

The saturation temperature at the interface between the steam and water film is solved by the Colburn–Hougen diffusion calculation [21, 22].

3 Results and discussions

3.1 Experimental apparatus

The results from MIT insurge experiments were used to verify the steam–gas pressurizer model in this study. The experimental apparatus is shown in Fig. 2. The test facility essentially consisted of two stainless-steel tanks, an insurge line, and a gas-injection system. The primary tank, which models the pressurizer volume, is a 203.2-mm-inner-diameter pipe and is 1143 mm in height. The storage tank is filled with $\sim 20^\circ\text{C}$ water pressurized with nitrogen. The noncondensable-gas-injection line is in the bottom of the primary tank.

In conjunction with the $\sim 20^\circ\text{C}$ insurge water, the operating pressure in the primary tank was brought up to approximately 0.53 MPa. Steam was bubbled through the primary tank to assist the heaters in bringing the tank up to saturation conditions. After the tank reached saturation, the steam line was isolated, and then, the noncondensable gas was injected into the vapor space after the primary tank had been purged of other dissolved gases, and before the system had reached operating pressure. In order to reduce local density gradients in the primary tank during the injection of a noncondensable gas, the process of injection was carried out as slowly as possible. The system was then brought up to about 0.53 MPa with the noncondensable gas already introduced into the primary tank.

When the tank reached operating pressure and the system was at thermal equilibrium, the saturation conditions in the tank were maintained by immersion heaters; the heaters were turned off when the insurge was initiated. Before the insurge experiment began, the initial water level in the primary tank was kept at 413.8 mm. The insurge was then initiated by opening the quick-opening valve at the base of the pressurizer; the insurge rate was approximately 0.4 kg/s.

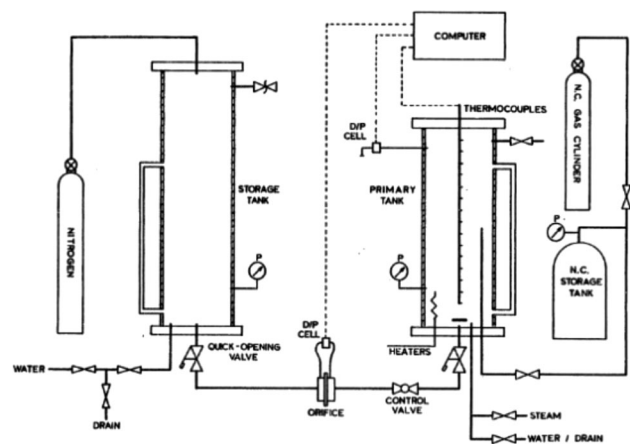


Fig. 2 Schematic of MIT experimental insurge apparatus

Based on the MIT experimental apparatus and conditions, the nodes of the experimental system are shown in Fig. 3. The following simplifications were made in Relap5 model: The storage tank was represented by a time-dependent volume component, designated the 110 card, and the valve and pipe between the primary tank and storage tank were represented by a time-dependent junction component, designated the 120 card, to regulate the insurge flow rate. The primary tank was modeled as a pipe component, designated the 108 card. The primary tank and heat structure were divided into ten control volumes, which was the best choice based on a sensitivity analysis.

During the simulation, the initial condition in the 110 card was set to 20 °C and the insurge rate, 0.4 kg/s, was set in the 120 card. The primary tank, the 108 card, was filled with water to a level of 413.8 mm and vapor with non-condensable gas. The mass fraction of and type of non-condensable gas was changed during the simulation, and the heat structure was used to simulate the environmental heat loss, 1.3 kW. The calculations were performed using Relap5, and nitrogen and argon were chosen as the non-condensable gases for modeling.

3.2 Results

Figure 4 shows the calculation results without a non-condensable gas in the pressurizer. The initial pressure in the primary tank was 0.531 MPa. Upon the insurge flow entering the primary tank, the pressure in the pressurizer changed significantly. The peak pressure was 0.647 MPa

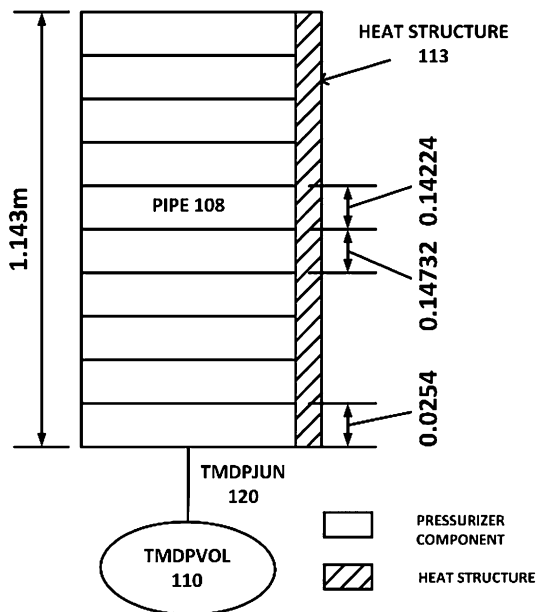


Fig. 3 Grids of experimental system

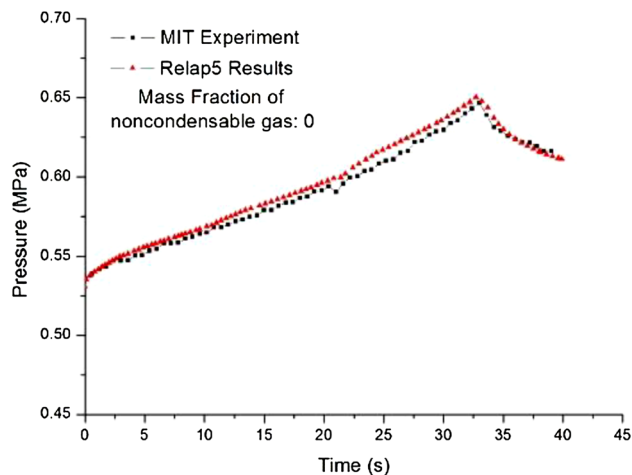


Fig. 4 Pressure transient without noncondensable gas

when the insurge ended. Subsequently, the pressure in the pressurizer decreased because of the energy dissipation.

Inspection of Fig. 4 indicates that the calculations of the model in this study are in excellent agreement with the experimental results when there is no noncondensable gas in the pressurizer; the maximum error in the calculation is 0.8%. Thus, the model can accurately predict the pressure in the pressurizer without a noncondensable gas.

The distribution of temperature in the pressurizer is shown in Fig. 5. Since the insurge water temperature was 20 °C, which was significantly cooler than the initial temperature in the pressurizer, thermal stratification occurs as is shown in the figure. The liquid region (at 0.0254, 0.1676, and 0.5740 m) in the pressurizer experienced an obvious change in temperature.

The steam/gas region (at 1.00 m) exhibited a very small temperature variation. The temperature change became smaller with increasing height, and the largest temperature

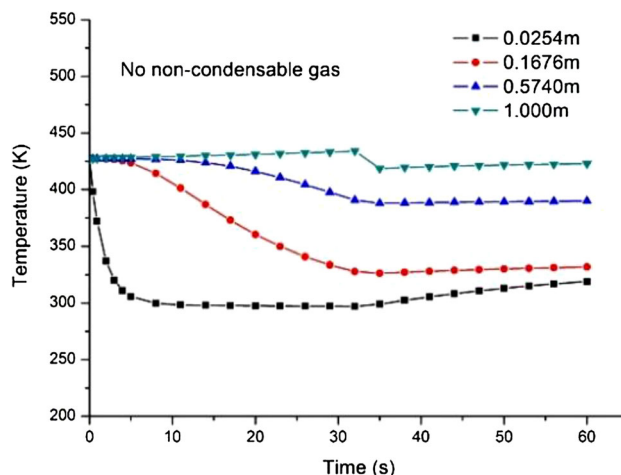


Fig. 5 Distribution of temperature at different positions

drop (approximately 125 °C) occurred in the bottom of the primary tank. It is easily found from inspection of Fig. 5 that there was an abrupt temperature drop at 1.00 m. Owing to the insurge of water, the pressure in the steam–gas pressurizer will increase, and then, the temperature will also increase with the change of pressure because of the saturation conditions in the steam/gas region. An abrupt drop in pressure will occur when the insurge ends (after approximately 33 s, as shown in Fig. 5), so the saturation temperature will decrease abruptly as well, also shown in Fig. 5.

The calculation results for different mass fractions of nitrogen are shown in Fig. 6. The change of pressure in the pressurizer is apparently different when the mass fraction of nitrogen varies, and the peak pressure increases with the increase in nitrogen mass fraction. The peak pressure ranged from 0.71 to 1.045 MPa when the mass fraction of nitrogen ranged from 3 to 20%. This is due to the condensation heat transfer in the presence of a noncondensable gas, which decreases the heat-transfer coefficient with increasing mass fraction of a noncondensable gas. We note that the Relap5 model calculations have same development tendency as the experimental results when the nitrogen mass fraction varies, while the calculation errors are different.

For 3% N₂, the Relap5 model performs much better, and the predicted and experimental values are in excellent agreement with each other and the errors are rather small. For 10 and 20% N₂, the calculation accuracy after the peak pressure is reached becomes worse but still tolerable, with the maximum error being approximately 13.1% at a time of 45 s for 10% N₂. However, the model can accurately predict the pressure change before the insurge ends, and the peak pressures are therefore able to be calculated accurately.

The pressure transients in the pressurizer when the noncondensable gas is argon are shown in Fig. 7, which indicates that the model gives good calculation accuracy

for small mass fractions of argon. As expected, as the argon mass fraction increases, the errors of the Relap5 model also increase. The peak pressure values are well predicted, but after reaching peak pressure the pressure values predicted by the Relap5 model tend to be smaller compared to experimental values; the maximum error is 10%.

It can be realized from Figs. 6 and 7 that the pressure transients can be predicted accurately by the Relap5 model developed for this study, especially for the pressurizer's peak pressure. The pressure transients in the pressurizer are very different for different types of noncondensable gas. As shown in Fig. 8, there is an obvious difference between nitrogen and argon with the same mass fraction (10%). The pressure in the presence of nitrogen is always larger than that in the presence of argon, and the peak pressure difference reached 0.068 MPa in our experiment. The difference in peak pressure is caused by the degradation of condensation heat transfer due to the different types of noncondensable gas, either nitrogen or argon. It is easily seen that the pressure for nitrogen will always be larger than that of argon at other mass fractions.

Comparing the Relap5 model calculations with the experimental values, it can be seen that the noncondensable gas plays a key role in the pressure transient process in the steam–gas pressurizer, and it is therefore necessary to consider the effect of the noncondensable gas in the steam–gas pressurizer model. Indeed, even a small amount of noncondensable gas can considerably reduce the condensation heat transfer near the wall. In this study, a modification factor f_c for the wall condensation model was introduced to evaluate the effect of a noncondensable gas on the heat- and mass-transfer processes during vapor condensation near the wall. However, this method sometimes seems a little rough and the model's calculation accuracy may be unsatisfactory but still tolerable when the mass fraction of the noncondensable gas is large.

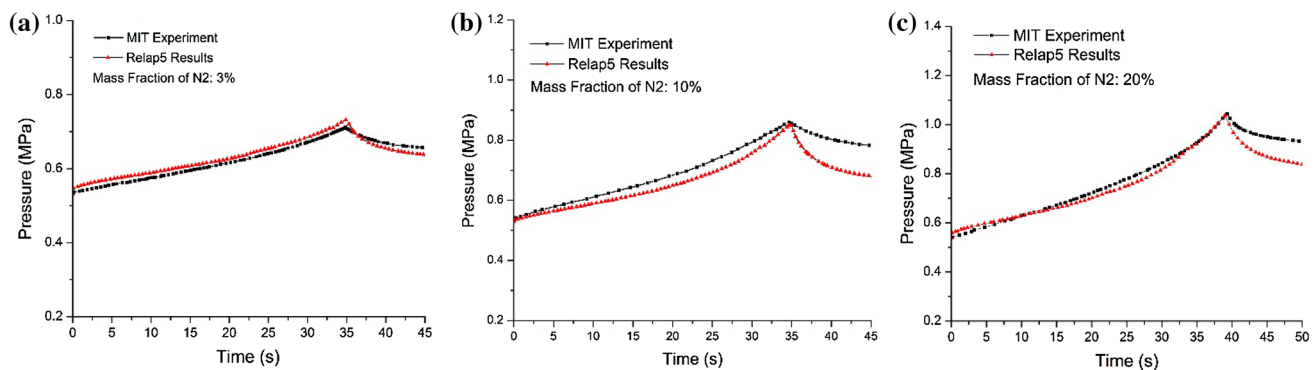


Fig. 6 Pressure transients of N₂

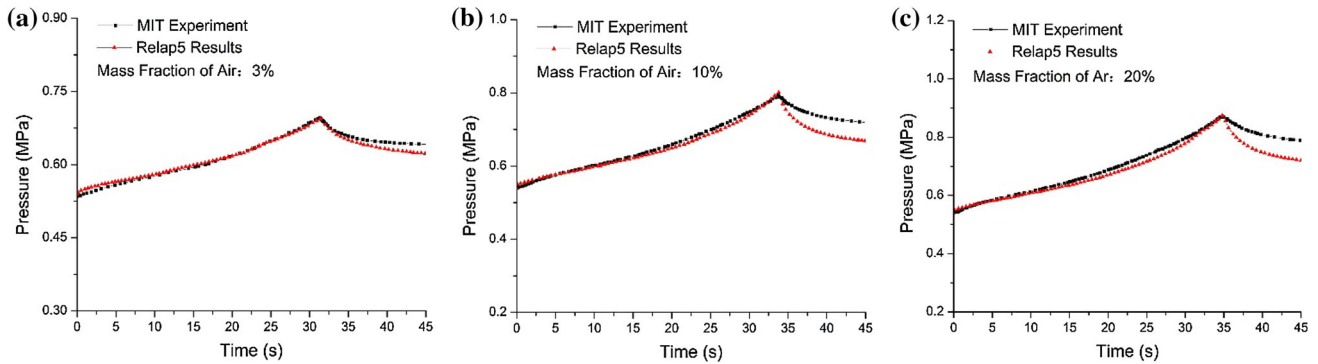


Fig. 7 Pressure transients of Ar

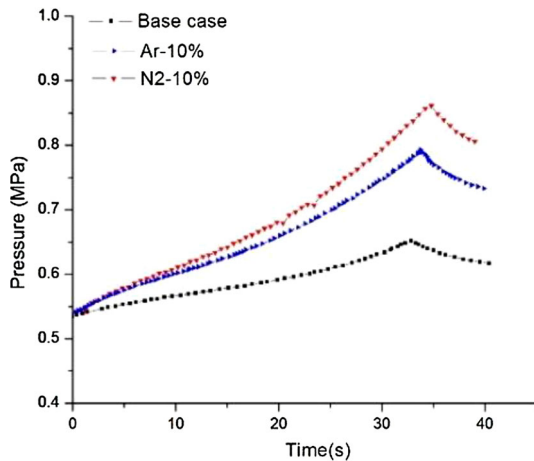


Fig. 8 Comparison of pressures with N_2 and Ar

4 Conclusions

In this study, a steam–gas pressurizer model was developed based on Relap5 code and verified using the results of MIT insurge experiments. The model well predicted the pressure transient in the steam–gas pressurizer, and the effect of a noncondensable gas on the condensation near the wall was considered under different experimental conditions. When the mass fraction of the noncondensable increased, the peak pressure increased considerably. At the same time, the pressure change process may be different due to different types of noncondensable gas.

References

1. Y.J. Zhang, X.Z. Wang, Development progress and prospect for industrial application of the 200 MW low temperature nuclear heating reactor. *Nucl. Power Eng.* **24**(2), 180–183 (2003). (in Chinese)
2. O.B. Samoilov, A.V. Kurachenkov, Nuclear district heating plants AST-500. *Nucl. Eng. Des.* **173**(1), 109–117 (1997). doi:10.1016/S0029-5493(97)00087-3
3. T.-W. Kim, J.-W. Kim, G.-C. Park, Development of nonequilibrium pressurizer model with noncondensable gas. *Nucl. Eng. Des.* **236**(4), 375–384 (2006). doi:10.1016/j.nucengdes.2005.09.003
4. M.T. Leonard, P. Griffith, The effects of a noncondensable gas on pressurizer insurge transients (1984). http://www.researchgate.net/publication/37600723_The_effects_of_a_noncondensable_gas_on_pressurizer_insurg_transients
5. S.N. Kim, P. Griffith, PWR pressurizer modeling. *Nucl. Eng. Des.* **102**(2), 199–209 (1987). doi:10.1016/0029-5493(87)90253-6
6. M. Murase, Y. Kataoka, T. Fujii, Evaporation and condensation heat transfer with a noncondensable gas present. *Nucl. Eng. Des.* **141**(1), 135–143 (1993). doi:10.1016/00295493(93)9098-T
7. T.W. Kim, Development of steam–gas pressurizer model based on two-region nonequilibrium with noncondensable gas. Ph.D. thesis, Seoul National University, Korea, 2005
8. G. Espinosa-Paredes, A.N. Ez-Carrera, SBWR model for steady-state and transient analysis. *Sci. Technol. Nucl. Install.* **01**, 1–18 (2008). doi:10.1155/2008/428168
9. G. Espinosa-Paredes, A. Nuñez-Carrera, A. Vazquez-Rodriguez, Simplified distributed parameters BWR dynamic model for transient and stability analysis. *Ann. Nucl. Energy* **33**(33), 1245–1259 (2006). doi:10.1016/j.anucene.2006.08.009
10. G. Espinosa-Paredes, J. Alvarez-Ramirez, A. Nunez-Carrera et al., Dynamic comparison of three and four-equation reactor core models in a full-scope power plant training simulator. *Nucl. Technol.* **145**(2), 150–162 (2004). http://www.ans.org/pubs/journals/nt/a_3466
11. S.M. Baek, H.C. No, I.Y. Park, A nonequilibrium three-region model for transient analysis of pressurized water reactor pressurizer. *Nucl. Technol.* **74**(3), 260–266 (1986). http://www.ans.org/pubs/journals/nt/a_33828
12. C.Q. Yan, *Two Phases Flow*. (Harbin Engineering University Press, Harbin (China), 2010), pp. 30–38. (in Chinese)
13. S. Patankar, *Numerical Heat Transfer and Fluid Flow* (CRC Press, Boca Raton, 1980), pp. 41–109
14. J.H. Lienhard, *A Heat Transfer textbook* (CourierCorporation, North Chelmsford, 2013), pp. 399–416
15. G. Espinosa-Paredes, O. Cazarez-Candia, A. Vazquez, Theoretical derivation of the interaction effects with expansion effects to bubbly two-phase flows. *Ann. Nucl. Energy* **31**(2), 117–133 (2004). doi:10.1016/S0306-4549(03)00218-4
16. G. Espinosa-Paredes, A. Nuñez-Carrera, E.J. Martinez-Mendez, Interaction forces model on a bubble growing for nuclear best estimate computer codes. *Ann. Nucl. Energy* **32**(14), 1546–1566 (2005). doi:10.1016/j.anucene.2005.04.002
17. F.J. Valdes-Parada, G. Espinosa-Paredes, Darcy’s law for immiscible two-phase flow: a theoretical development. *J. Porous Media* **8**, 557–567 (2005). doi:10.1615/JPorMedia.v8.i6.20

18. M.M. Shah, A general correlation for heat transfer during film condensation inside pipes. *Int. J. Heat Mass Transf.* **22**(4), 547–556 (1979). doi:[10.1016/0017-9310\(79\)90058-9](https://doi.org/10.1016/0017-9310(79)90058-9)
19. K.Y. Lee, M.H. Kim, Experimental and empirical study of steam condensation heat transfer with a noncondensable gas in a small-diameter vertical tube. *Nucl. Eng. Des.* **238**(1), 207–216 (2008). doi:[10.1016/j.nucengdes.2007.07.001](https://doi.org/10.1016/j.nucengdes.2007.07.001)
20. K.M. Vierow, V.E. Schrock, Condensation in a natural circulation loop with noncondensable gases, 1, in *Proceedings of the International Conference on Multiphase Flows' 91*, Tsukuba, Japan, 1991
21. A.P. Colburn, O.A. Hougen, Design of cooler condensers for mixtures of vapors with noncondensing gases. *Ind. Eng. Chem.* **26**(11), 1178–1182 (1934). doi:[10.1021/ie50299a011](https://doi.org/10.1021/ie50299a011)
22. K.E. Carlson, R.A. Riemke, S.Z. Rouhani et al., *RELAP5/MOD3 Code Manual Volume I: Code Structure, System Models and Solution Methods*. US NRC NUREG/CR-5535, 1990